Experimental and Molecular Pathology xxx (2014) xxx–xxx

Contents lists available at ScienceDirect

Experimental and Molecular Pathology

journal homepage: www.elsevier.com/locate/yexmp

Inhibition of p300 suppresses growth of breast cancer. Role of p300 subcellular localization

Q3 María E. Fermento [a,1], Norberto A. Gandini [a,1], Débora G. Salomón [a], María J. Ferronato [a], Cristian A. Vitale [b], Julián Arévalo [c], Alejandro López Romero [d], Myriam Nuñez [e], Manfred Jung [f], María M. Facchinetti [a], Alejandro C. Curino [a,*]

[a] Laboratorio de Biología del Cáncer, Instituto de Investigaciones Bioquímicas Bahía Blanca, Centro Científico Tecnológico (INIBIBB-CCT-CONICET), Camino La Carrindanga Km. 7, 8000 Bahía Blanca, Argentina
[b] Departamento de Química, Instituto de Química del Sur (INQUISUR-CONICET), Universidad Nacional del Sur, Av. Alem 1253, 8000 Bahía Blanca, Argentina
[c] Servicio de Patología del Hospital Interzonal General de Agudos Dr. José Penna, Av. Lainez 2401, 8000 Bahía Blanca, Argentina
[d] Departamento de Hematología, IACA, San Martín 68, 8000 Bahía Blanca, Argentina
[e] Cátedra de Matemática, Departamento de Físico-Matemática, Facultad de Farmacia y Bioquímica, Universidad de Buenos Aires, Viamonte 444, C1053ABJ Ciudad autónoma de Buenos Aires, Argentina
[f] Institute of Pharmaceutical Sciences, Albert-Ludwigs University Freiburg, Albertstrasse 25, 79104 Freiburg, Germany

ARTICLE INFO

Article history:
Received 5 September 2014
Accepted 12 September 2014
Available online xxxx

Keywords:
p300
Breast cancer
Cell line
Animal model
Human biopsies

ABSTRACT

There is evidence that p300, a transcriptional co-factor and a lysine acetyl-transferase, could play a role both as an oncoprotein and as a tumor suppressor, although little is known regarding its role in breast cancer (BC). First we investigated the role p300 has on BC by performing pharmacological inhibition of p300 acetyl-transferase function and analyzing the effects on cell count, migration and invasion in LM3 murine breast cancer cell line and on tumor progression in a syngeneic murine model. We subsequently studied p300 protein expression in human BC biopsies and evaluated its correlation with clinical and histopathological parameters of the patients. We observed that inhibition of p300 induced apoptosis and reduced migration and invasion in cultured LM3 cells. Furthermore, a significant reduction in tumor burden, number of lung metastases and number of tumors invading the abdominal cavity was observed in a syngeneic tumor model of LM3 following treatment with the p300 inhibitor. This reduction in tumor burden was accompanied by a decrease in the mitotic index and Ki-67 levels and an increase in Bax expression. Moreover, the analysis of p300 expression in human BC samples showed that p300 immunoreactivity is significantly higher in the cancerous tissues than in the non-malignant mammary tissues and in the histologically normal adjacent tissues. Interestingly, p300 was observed in the cytoplasm, and the rate of cytoplasmic p300 was higher in BC than in non-tumor tissues. Importantly, we found that cytoplasmic localization of p300 is associated with a longer overall survival time of the patients.

In conclusion, we demonstrated that inhibition of the acetylase function of p300 reduces both cell count and invasion in LM3 cells, and decreases tumor progression in the animal model. In addition, we show that the presence of p300 in the cytoplasm correlates with increased survival of patients suggesting that its nuclear localization is necessary for the pro-tumoral effects.

Abbreviations: BC, breast cancer; CREB, cAMP responsive element binding protein; DMSO, dimethylsulfoxide; VV56, 2-(3-(3,4-dichlorobenzyloxy)phenoxy)pentadecanoic acid; VV59, 2-(3-(3,4-dichlorobenzyloxy)phenoxy)hexadecanoic acid; DMEM, Dulbecco's modified Eagle's medium; FBS, Fetal Bovine Serum; PBS, phosphate buffered saline; WB, western blot; IF, immunofluorescence; BSA, bovine serum albumin; PI, propidium iodide; ECL, enhanced chemiluminescence; SC, subcutaneously; PFA, paraformaldehyde; H&E, hematoxylin and eosin; IHC, Immunohistochemistry; IRS, Immuno-Reactive-Score; AV, annexin V; NAT, normal adjacent tissues; HAT, hyperplastic adjacent tissues; ER, estrogen receptor; PR, progesterone receptor; Her2, human epidermal growth factor receptor 2; SVG, status of overall survival; HDAC, histone deacetylase; T, tumor.

* Corresponding author at: Laboratorio de Biología del Cáncer, Instituto de Investigaciones Bioquímicas Bahía Blanca (INIBIBB-CONICET), Centro Científico Tecnológico Bahía Blanca, Camino La Carrindanga Km. 7, C.C. 857, 8000 Bahía Blanca, Argentina.
E-mail addresses: efermento@criba.edu.ar (M.E. Fermento), ngandini@uns.edu.ar (N.A. Gandini), dsalomon@criba.edu.ar (D.G. Salomón), jferronato@criba.edu.ar (M.J. Ferronato), cvitale@criba.edu.ar (C.A. Vitale), arevalo_julian@hotmail.com (J. Arévalo), hematologia@iaca.com.ar (A. López Romero), myr1710@yahoo.com (M. Nuñez), manfred.jung@pharmazie.uni-freiburg.de (M. Jung), facchinm@criba.edu.ar (M.M. Facchinetti), acurino@criba.edu.ar (A.C. Curino).
[1] These authors contributed equally to this work.

http://dx.doi.org/10.1016/j.yexmp.2014.09.019
0014-4800/© 2014 Published by Elsevier Inc.

1. Introduction

Breast cancer (BC) is the most frequently diagnosed malignant neoplasia and a leading cause of cancer death in females worldwide (Jemal et al., 2011). It is not a single disease but instead constitutes a variety of lesions with distinct cellular origins, somatic changes, and etiologies (Lanari et al., 2012). In addition, BC patients with the same diagnostic and clinical prognostic profile can have markedly different clinical outcomes. This difference is possibly caused by the limitation of our current taxonomy of BCs, which groups molecularly distinct diseases into clinical classes based mainly on morphology (Sotiriou et al., 2003). This reflects the need to find new molecular markers to assist in the diagnosis, prognosis and treatment of this type of cancer.

Transcriptional coactivator p300 participates in the regulation of a wide range of biological processes such as proliferation, cell cycle regulation, apoptosis, differentiation, senescence and DNA damage response (Chan and La Thangue, 2001; Giles et al., 1998; Giordano and Avantaggiati, 1999; Goodman and Smolik, 2000). This protein functions primarily as a transcription cofactor for a number of nuclear proteins including known oncoproteins such as Jun, Fos, and E2F and for tumor-suppressor proteins such as p53, Rb, Smads, and BRCA1 (Avantaggiati et al., 1997; Chan and La Thangue, 2001; Tomita et al., 2000). In addition, it functions as histone acetyltransferase (Bannister and Kouzarides, 1996; Ogryzko et al., 1996) and is capable of acetylating a number of non-histone proteins, including p53, p73, Rb, E2F, Myb, MyoD, HMG(I) Q4 Y, GATA1 and alpha-importin (Bannister and Miska, 2000; Chan and La Thangue, 2001; Costanzo et al., 2002; Tomita et al., 2000).

An increasing body of evidence indicates that p300 may be important in cancer (Iyer et al., 2004). Nonetheless, the role of the protein in this disease remains unclear, since there is evidence indicating that it can function both as a tumor suppressor and as an oncoprotein (Goodman and Smolik, 2000). In this regard, it has been reported that increased expression of p300 correlates with cancer progression and decreased patient survival (Debes et al., 2003; Gao et al., 2014; Ishihama et al., 2007; M. Li et al., 2011; Y. Li et al., 2011; Syrjänen et al., 2010). Contrariwise, it has also been described that p300 overexpression predicted a favorable patient outcome (Huh et al., 2013). Interestingly, decreased expression of nuclear p300 protein levels was associated with disease progression and worse prognosis of melanoma patients (Rotte et al., 2013). Furthermore, the mechanisms that regulate the activity of p300 have not yet been elucidated, although many reports point to the importance of the intracellular localization of p300 Q5 for its activity (J. Chen et al., 2007; Y. Chen et al., 2007; Mackeh et al., 2014; Sebti et al., 2014; Shi et al., 2009).

To our knowledge there is only one report showing the association of p300 expression with tumor recurrence and prognosis of breast cancer patients (Xiao et al., 2011) and no investigations that explore the role of the subcellular localization of p300 in BC progression. In this study we present the first findings to investigate the mechanisms through which p300 influences BC progression evaluating the possibility that p300 and its subcellular localization can be important factors in the progression of this disease.

2. Materials and methods

2.1. Reagents

Curcumin (C.I.75300, Biopack), a novel p300/cAMP responsive element binding (CREB) protein specific inhibitor of acetyltransferase (Balasubramanyam et al., 2004; Y. Chen et al., 2007) was dissolved in dimethyl sulfoxide (DMSO, Sigma) to produce a 200 mM stock solution. 2-(3-(3,4-Dichlorobenzyloxy)phenoxy)pentadecanoic acid (VV56 or Cpd 4k) and 2-(3-(3,4-dichlorobenzyloxy)phenoxy)hexadecanoic acid (VV59 or Cpd 4l), inhibitors of p300 acetyl-transferase activity (Eliseeva et al., 2007) were dissolved in DMSO to produce a 100 mM stock solution.

2.2. Cell culture

LM3 is a tumor cell line derived from a murine mammary adenocarcinoma that spontaneously arose in BALB/c mice (Urtreger et al., 1997) and was a generous gift from E. Bal de Kier Joffé (Instituto de Oncología Ángel Roffo, Buenos Aires, Argentina). Cells were maintained in Dulbecco's modified Eagle's medium (DMEM, Sigma) supplemented with 5% (v/v) Fetal Bovine Serum (FBS, Gibco), L-glutamine (5 mM, Gibco), penicillin (Gibco, 100 U/ml), and streptomycin (Gibco, 100 μg/ml) at 37 °C in a humidified 5% CO_2 air atmosphere.

2.3. Cell count

The cells were plated at a density of 1500 cells/well into 96 multi-well dishes in complete medium. They were treated with 25, 50, 75 and 100 μM of VV56, VV59 or vehicle (DMSO) for 12, 24, 48, and 72 h. They were washed with phosphate buffered saline (PBS) 1×, trypsinized, suspended in 100 μl complete medium and counted manually using a hemocytometer, as previously described (Gandini et al., 2014). Additionally, cell viability was assessed by the WST colorimetric assay (Roche). For this purpose, following treatment with p300 inhibitor, the cells were incubated for 1 h at 37 °C with the tetrazolium salt WST-1 (4-[3-(4-Iodophenyl)-2-(4-nitrophenyl)-2H-5-tetrazolio]-1,3-benzene disulfonate) and the absorbance of the formazan product was read at 450 nm. The results were depicted as percentage of vehicle-treated cells.

2.4. Cell migration

Cell migration was studied by employing the "wound healing" assay as previously described (Petit et al., 2000). Briefly, the cells were seeded in 35 mm Petri dishes and cultured until confluence. The cells were treated with VV59 (12.5 μM), VV56 (12.5 μM) or DMSO and they were scraped with a 200 μl micropipette tip, denuding a strip of the monolayer. Then they were observed and photographed every 4 h for

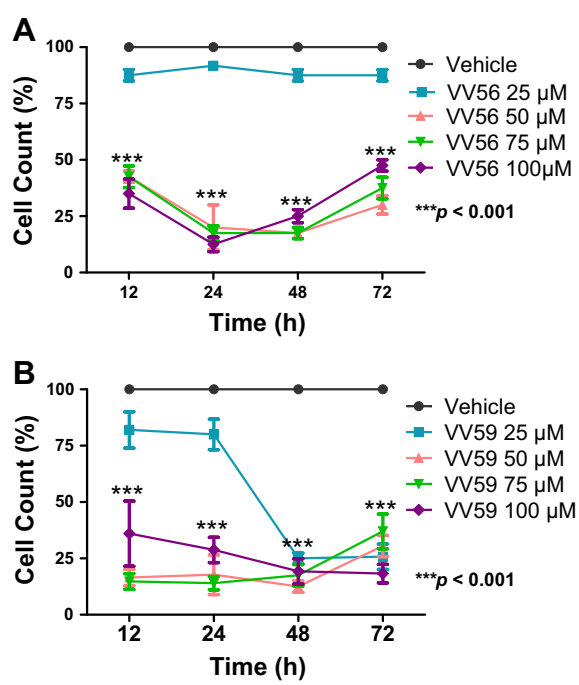

Fig. 1. p300 inhibition decreases LM3 cell count. Cell count was assessed in LM3 cells following different concentrations and times of VV56 (A) or VV59 (B). Concentrations and times used were 25, 50, 75, 100 μM and 12, 24, 48 and 72 h, respectively. Data show the percentage of cells in relation to vehicle-treated cells and are the means (±SD) of triplicate experiments; $p < 0.001$, from Anova test.

Please cite this article as: Fermento, M.E., et al., Inhibition of p300 suppresses growth of breast cancer. Role of p300 subcellular localization, Exp. Mol. Pathol. (2014), http://dx.doi.org/10.1016/j.yexmp.2014.09.019

24 h. Images were captured with an inverted microscope (Nikon Eclipse TE2000-S), equipped with a digital camera (Nikon Coolpix S4, 6.0 Mpix, 10× zoom). The uncovered wound area was measured and quantified at different intervals for 24 h with ImageJ 1.37v (NIH).

2.5. Cell invasion

LM3 cells were used in invasion assays through Matrigel chambers as described previously (Gueron et al., 2009). In brief, cell suspensions treated with VV59 (12.5 μM) or DMSO (12,500 cells/well in 0.5 ml DMEM medium) were plated into 24-well inserts (Falcon cell culture inserts, 8 μm pore size) with Matrigel (BD). The lower chamber was filled with 0.6 ml of DMEM containing 5% (v/v) FBS (Gibco). After incubation for 12 h at 37 °C, the cells on the upper side of the transwell membrane were removed by cotton swab and rinsed with PBS 1×. Cells migrating to the lower side of the membrane were fixed in 4% paraformaldehyde (PFA) for 20 min at room temperature, stained with crystal violet (Sigma), photographed, and counted.

2.6. Fluorescence and confocal imaging

Immunofluorescence (IF) was performed as previously described (Gandini et al., 2012). Briefly, LM3 cells were seeded on glass coverslips in 35 mm Petri dishes and cultured until 50% confluence. They were treated with VV59 (12.5 μM) for 12 h. After treatment, they were washed three times with PBS 1× and fixed with PFA 4% in PBS 1×. The cells were then permeabilized with 0.2% triton in PBS 1× and blocked with 1% bovine serum albumin (BSA) in PBS 1×. Then they were incubated with rhodamine–phalloidin (1:1000) in 2% BSA in PBS 1× for 1 h. After that they were washed with PBS 1× and DAPI (1:10,000). Glass coverslips were mounted on glass microscope slides, and confocal images were acquired with the Leica confocal microscopy TSP2 and analyzed with ImageJ 1.37v (NIH). The lamellipodia in the cells located at the edge of the colonies were counted by analyzing 10 images of 7–8 cells/field for each experimental point (Filigheddu et al., 2011). Also, to evaluate the expression of p300, rabbit polyclonal anti-p300 was used as the primary antibody (N-15 and C-20, sc-584 and 585, Santa Cruz Biotechnology, dilution: 1:100). After incubation with the primary antibody, the cells were incubated with anti-rabbit Alexa 566 fluoro-conjugated antibodies (Molecular Probes, Invitrogen). Then they were washed and mounted as already described. Counting of 200 cells in 400× random fields was done in order to study the proportion of cells containing p300 expression.

2.7. Cell cycle analysis

Cell cycle analysis was performed as previously described (Gandini et al., 2014). Briefly, LM3 cells treated with VV59 (50 μM) for 24 h

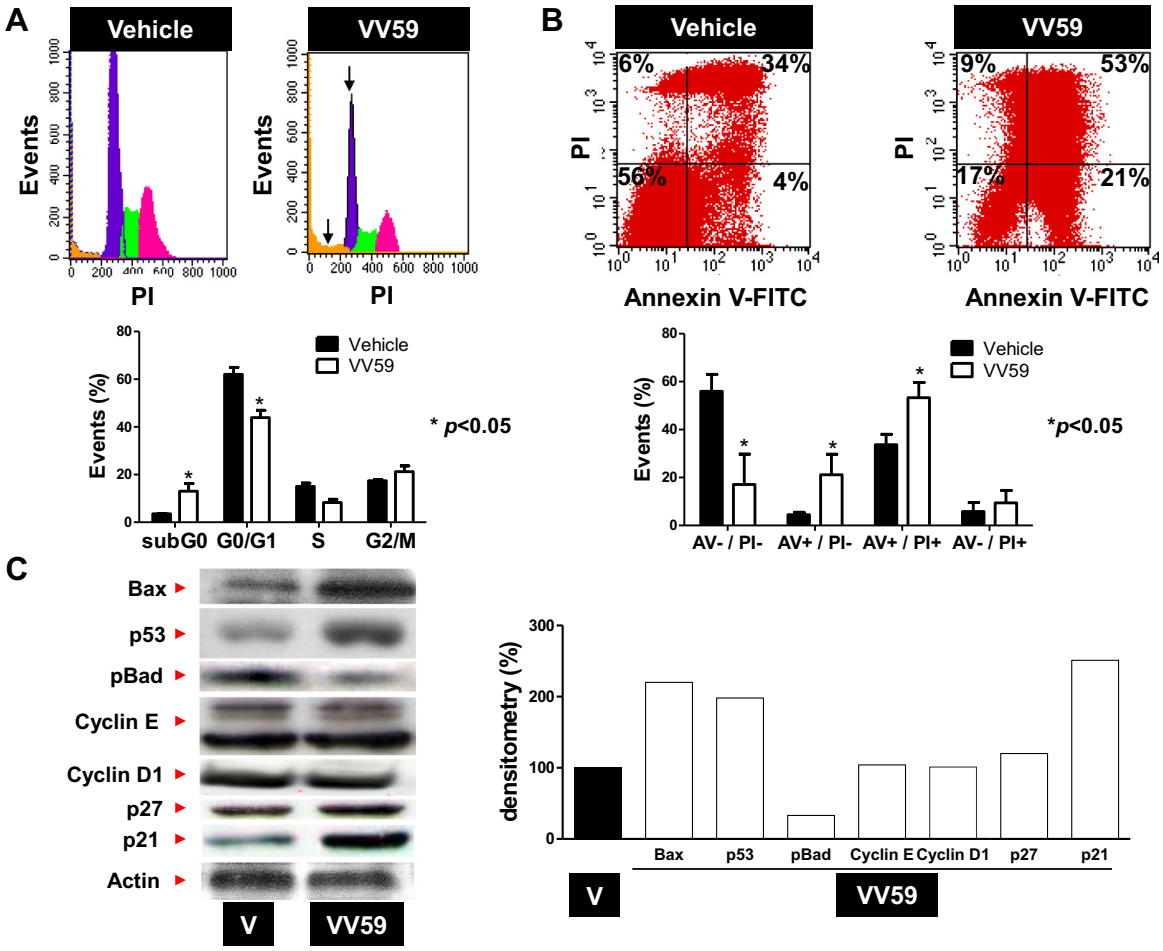

Fig. 2. p300 inhibition induces apoptosis in LM3 cells. A. Cell cycle analysis of LM3 cells treated with DMSO (vehicle) or VV59 (50 μM) for 24 h and assessed by flow cytometry. The percentages of sub-G0/G1 and G1 cell populations are indicated by arrows and plotted in a graph (below). B. Analysis of cellular apoptosis by Annexin V/PI staining. LM3 cells were treated with DMSO (vehicle) or VV59 (50 μM, 24 h), stained with FITC Annexin V and with PI and analyzed by flow cytometry. The graphic shows the quantification of cells in the early and late stages of apoptosis in one representative experiment; $p < 0.05$. C. Analysis of the levels of proteins involved in the regulation of apoptosis and cell cycle. LM3 cells were treated with VV59 (50 μM) for 18 h and cell lysates were subjected to WB analyses to detect Bax, p53, pBad, Cyclin E, Cyclin D1, p27 and p21. Protein loading was normalized with actin. The blots correspond to one representative experiment of three independent ones. The graph shows the densitometry of bands.

Please cite this article as: Fermento, M.E., et al., Inhibition of p300 suppresses growth of breast cancer. Role of p300 subcellular localization, Exp. Mol. Pathol. (2014), http://dx.doi.org/10.1016/j.yexmp.2014.09.019

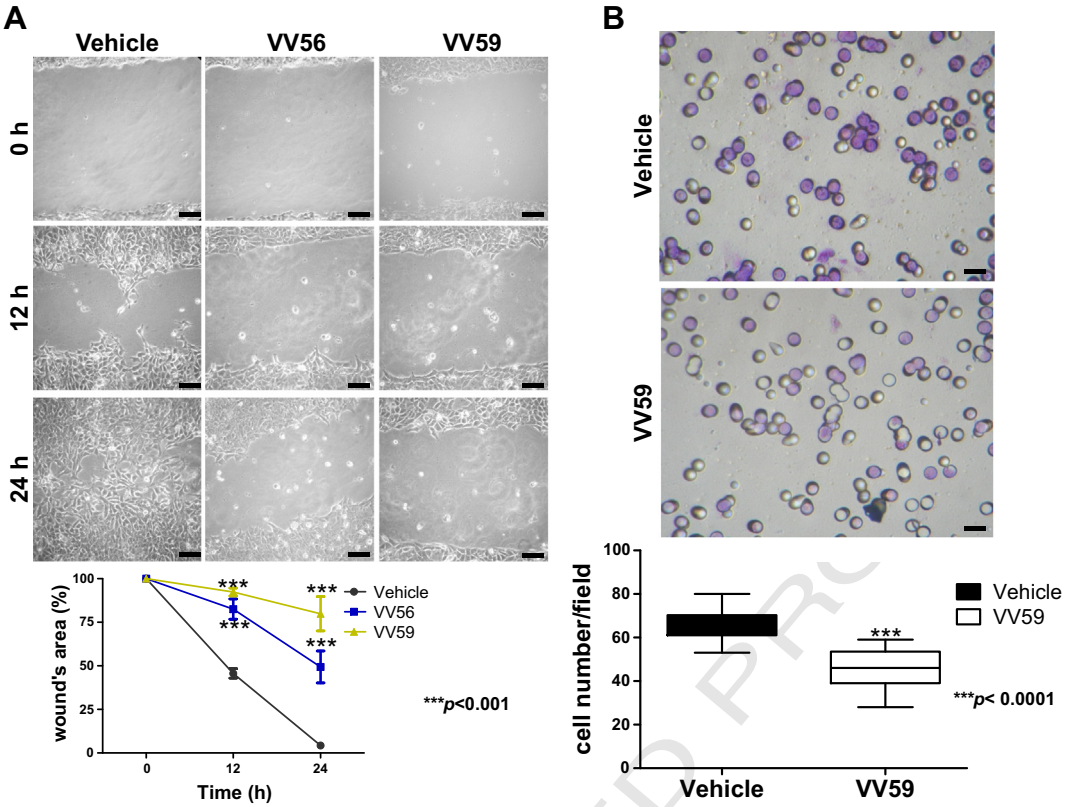

Fig. 3. p300 inhibition decreases migration and invasion rates of LM3 cells. A. Representative phase-contrast pictures of the wound-healing assay. LM3 cells were grown to confluence into a monolayer in 35 mm Petri dishes and treated with VV56 or VV59 (12.5 μM). A linear scratch wound was made along the culture plate, and cells were photographed at 0, 12 and 24 h following treatment. Representative pictures of three independent experiments are shown. The uncovered wound area was measured at 0, 12 and 24 h using ImageJ 1.37v software; objective 20×, *scale bars* represent 125 μm. The graph represents the mean percentage (±SD) of uncovered wound area taking the value at 0 h as 100%; $^{***}p < 0.001$, Anova test. B. LM3 cells were treated with DMSO (vehicle) or VV59 (12.5 μM) for 12 h and cell invasion was analyzed using Matrigel-coated transwell inserts. Cells that had invaded to the underside of the inserts after 12 h of incubation were stained with crystal violet and counted by light microscopy; objective 40×, *scale bars* represent 50 μm. Ten fields from each insert were counted. One representative picture from three independent experiments is shown ($p < 0.0001$; Student's t test).

were trypsinized, fixed with ice-cold 70% ethanol, stained with propidium iodide (PI, Roche), and analyzed for DNA content by FACScan Calibur Becton Dickinson. Data were analyzed by Cell Quest software (Becton Dickinson). At least 100,000 cells were analyzed for each sample.

2.8. Annexin V-FITC assay for apoptosis

Assay for apoptosis was performed as previously described (Gandini et al., 2014). The apoptosis assay was carried out with the Annexin V-FITC (AV, 556420) kit following the manufacturer's instructions (BD Biosciences). LM3 cells were treated with 50 μM of VV59 or vehicle (DMSO) for 24 h. Briefly, they were washed twice with cold PBS 1× and then were suspended in 1× binding buffer (10 mmol/l HEPES (pH 7.4), 150 mmol/l NaCl, 2.5 mmol/l $CaCl_2$) at a concentration of 1×10^6 cells/ml. Then, 100 μl of the solution was transferred to a 5 ml culture tube, and 5 μl of Annexin V-FITC (BD Pharmingen) and 10 μl of PI were added and incubated in the dark at room temperature. Apoptosis was quantified by flow cytometric analysis of Annexin V-FITC-PI-stained cells. Annexin V (+) and PI (−) cells were considered to be in early apoptosis and the percentage of this population of cells was calculated.

2.9. Western blot (WB)

Cells were seeded in plates with complete medium and treated with 50 μM of VV59 or vehicle (DMSO) for 4, 12, 18 and 24 h and then protein lysates were prepared according to previously described methods (Facchinetti et al., 2010). Briefly, 50 μg of protein was separated by SDS-PAGE on 12 and 15% gels, transferred onto nitrocellulose membrane, blocked with 5% non-fat dry milk for 30 min, then incubated with a primary antibody, washed, incubated further with horseradish peroxidase-conjugated secondary antibodies, and reactions were detected by enhanced chemiluminescence (ECL) following the manufacturer's directions (Amersham, ECL Plus Western Blotting Detection Reagents, GE Healthcare). Primary antibodies used were rabbit polyclonal anti-Bax (N-20) (Santa Cruz Biotechnology, sc-493), rabbit polyclonal anti-p300 (Santa Cruz Biotechnology, N-15 and C-20, sc-584 and 585), rabbit polyclonal anti-p53 (FL-393, Santa Cruz Biotechnologies, sc-6243), purified mouse anti-p21 (BD Biosciences, cat: 556430), purified mouse anti-p27(Kip1) (BD Biosciences, cat: 610241), anti-pBad, rabbit anti-cyclin D (Thermo Scientific, RM-9104-S1), and rabbit polyclonal anti-cyclin E (M-20, Santa Cruz Biotechnologies, sc-481). Anti-β-actin (C-11, polyclonal goat, Santa Cruz Biotechnologies, sc-1615) was used as internal control for protein loading and analysis.

2.10. Animal studies

In vivo studies were conducted in accordance with the NIH Guide for the Care and Use of Laboratory Animals. 3-month-old virgin female BALB/c mice, each weighing at least 20 g, were purchased from the Facultad de Ciencias Veterinarias (La Plata, Argentina). Animals were given free access to water and food, and were housed in a climate

Please cite this article as: Fermento, M.E., et al., Inhibition of p300 suppresses growth of breast cancer. Role of p300 subcellular localization, Exp. Mol. Pathol. (2014), http://dx.doi.org/10.1016/j.yexmp.2014.09.019

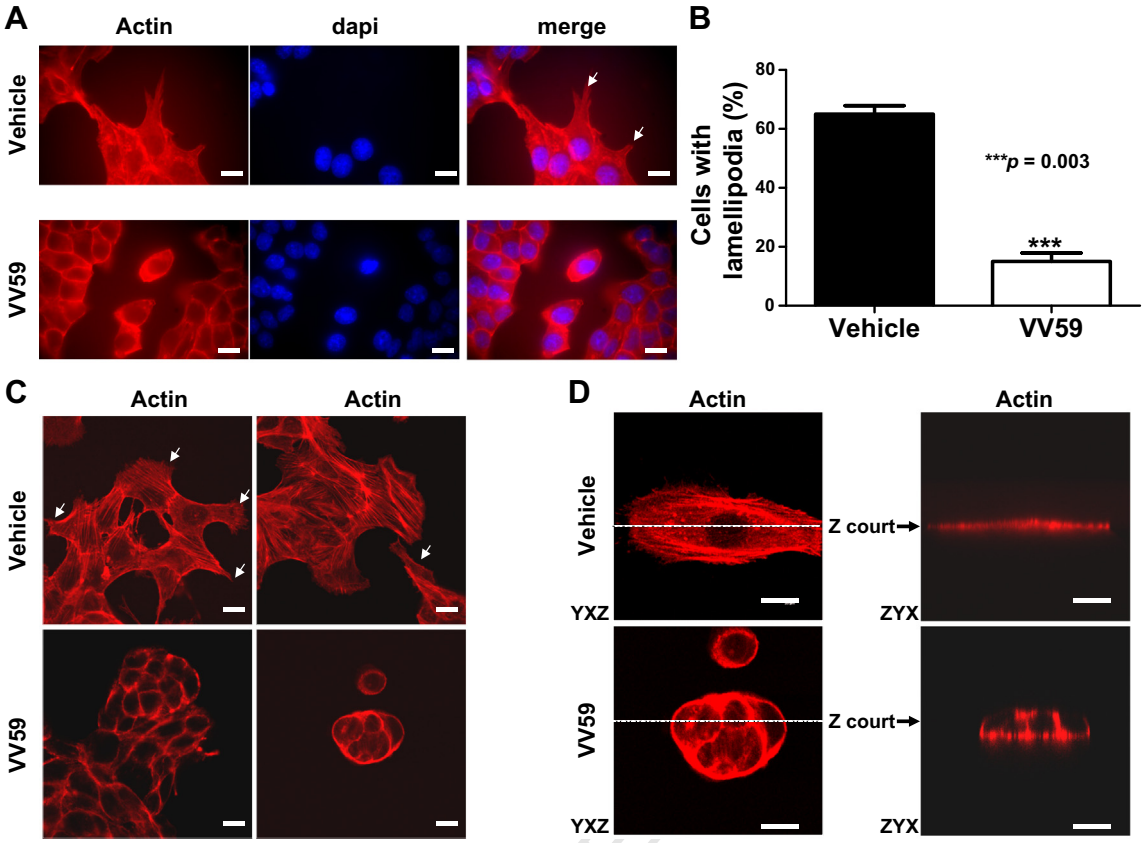

Fig. 4. p300 inhibition alters actin cytoskeleton in LM3 cells. LM3 cells were treated with DMSO (vehicle) or VV59 (12.5 μM). After 12 h, cells were fixed, stained, and images were acquired with a light (A) or confocal (C and D) fluorescence microscope. A. White arrow indicates a lamellipodium in cells with nuclei in blue (DAPI) and actin in red (phalloidin), objective 60×, *scale bars* represent 20 μm. B. Cells at the edge of colonies were scored for the presence of lamellipodia and these were counted. Ten images of 7–8 cells/field were acquired for each experimental point. Values are the mean ± SD of three independent experiments; $p = 0.003$, Student's t test. C. Confocal microscopy of phalloidin-stained cells. White arrows indicate lamellipodia in cells with actin in red (phalloidin), objective 63×, *scale bars* represent 20 μm. D. Confocal microscopy of phalloidin-stained cells showing Z court; objective 63×, electronic zoom 1.90, *scale bars* represent 20 μm. (For interpretation of the references to color in this figure legend, the reader is referred to the web version of this article.)

controlled room with a 12 h light/12 h dark cycle. 36 animals were injected subcutaneously (s.c.) with LM3 cells (4×10^5 cells in 100 μl of serum-free DMEM) in the right flank using a monojet 200, 30-gauge ×1/2 needle.

When tumors reached 50 to 70 mm^3 in volume, LM3 tumor-bearing mice were randomly divided in four groups and were injected as indicated previously (de Matos et al., 2012): 1) 6 mice with curcumin (50 mg/kg/in DMSO/serum-free DMEM), 2) 6 mice with vehicle of curcumin, 3) 12 mice with VV59 (45 mg/kg/in DMSO/serum-free DMEM), and 4) 12 mice with vehicle of VV59. Mice were injected three times a week for three weeks. Tumor growth was blindly measured daily with calipers and tumor volume was calculated as $\pi / 6 \times a \times b^2$, where a is the length in millimeters, and b is the width in millimeters. At the end animals were sacrificed by cervical dislocation. Tumors were then removed, weighed, measured and put into liquid nitrogen or PFA for further study. Tumor volume was calculated as $\pi / 6 \times a \times b \times c$, where a, b, and c are the three tumor dimensions. The organs were examined superficially for evidence of macroscopic metastasis and lungs were removed and fixed in Bouin's solution. The number of superficial lung metastases per mouse was counted by an investigator that was unaware of the sample assignment, with the aid of a Stereo Microscope (Nikon SMZ 1500). Peritoneum invasion was photographed and counted as previously described (Bruzzone et al., 2009).

Tumors and normal mammary glands were excised, bisected along the longest axis, fixed for 24 h in 4% PFA in PBS and processed into paraffin by standard procedures. In brief, after paraffin sections were dewaxed, they were rehydrated in a series of ethanol dilutions and either stained with hematoxylin and eosin (H&E) or used for immunohistochemical studies. Staining procedures were used to observe histopathological characteristics. Mitotic index was calculated as the number of the mitotic figures observed in 10 fields at a magnification of 400× in the H&E stained slides. The expression of p300 and the apoptotic and proliferation processes were studied by immunohistochemistry.

2.11. Human breast cancer samples

Formalin-fixed paraffin-embedded tissues from patients (ductal breast carcinomas, n = 101 and non-malignant mammary glands, n = 9) were retrieved from the pathology service of a local hospital, and their use was approved by the Commission for Medical Ethics and Clinical Studies. They were diagnosed as ductal breast cancer and further re-evaluated by our laboratory pathologist (JA). All tissue specimens were acquired at initial diagnosis from untreated patients and were classified morphologically and graded according to the current WHO system.

2.12. Immunohistochemistry (IHC)

IHC was performed as previously described (Facchinetti et al., 2010) [37]. IHC was carried out with the avidin–biotin complex immunoperoxidase technique. Four-μm sections of paraffin-embedded specimens were mounted on glass slides, deparaffinized with xylene, and rehydrated with graded alcohol. They were incubated for 10 min in 3% hydrogen peroxide in ethanol at 96 °C to quench endogenous peroxidase. After washing in PBS 1×, the sections were blocked for 30 min

Please cite this article as: Fermento, M.E., et al., Inhibition of p300 suppresses growth of breast cancer. Role of p300 subcellular localization, Exp. Mol. Pathol. (2014), http://dx.doi.org/10.1016/j.yexmp.2014.09.019

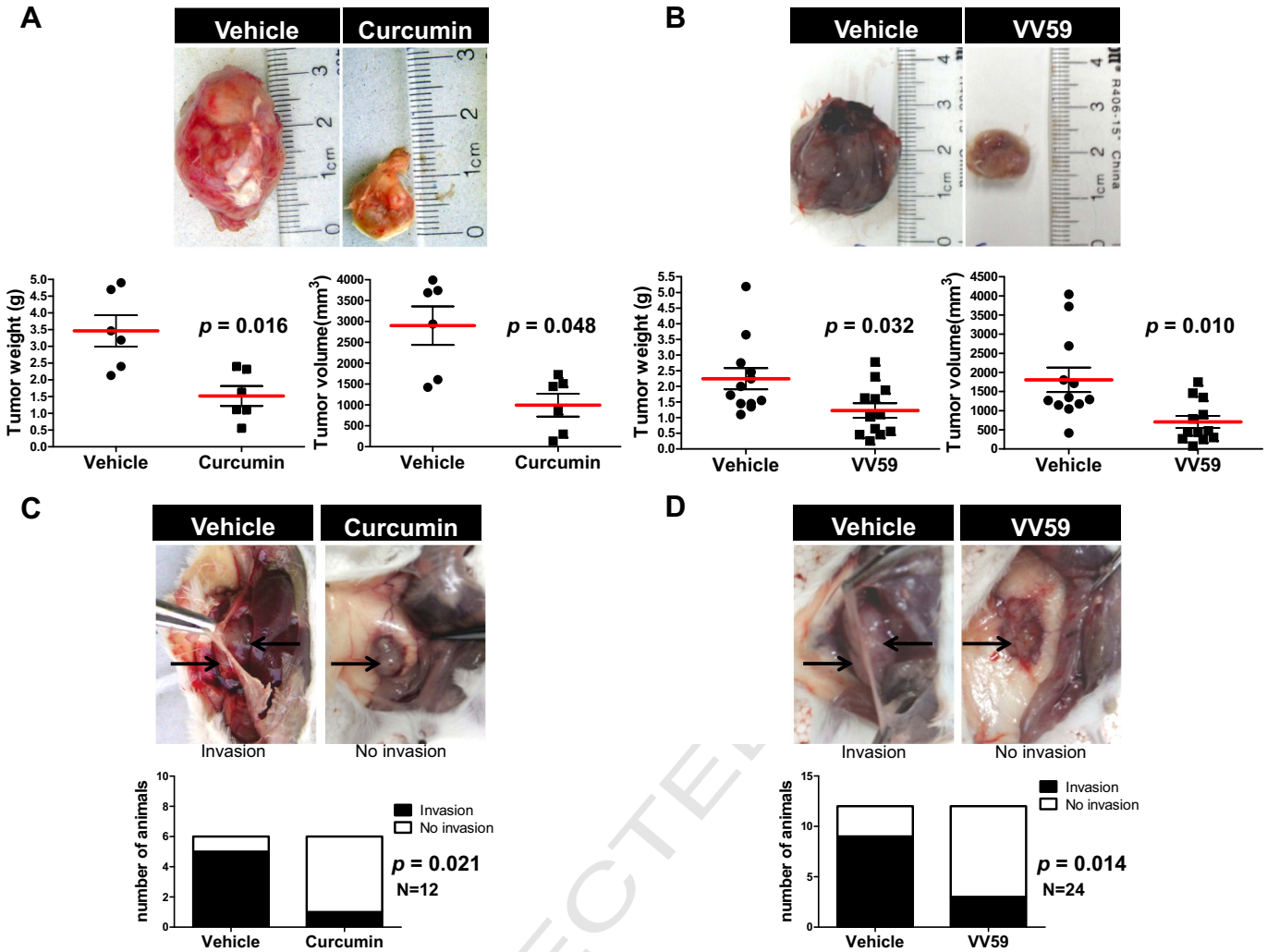

Fig. 5. p300 inhibition decreases tumor growth and invasion into the abdominal cavity in an animal model. LM3 cells (4×10^5) were inoculated subcutaneously in Balb-c mice. When the tumor reached 50 to 70 mm^3, curcumin (50 mg/kg in DMSO/serum free DMEM), VV59 (45 mg/kg in DMSO/serum free DMEM) or DMSO/serum free DMEM (control) was administered three times a week for three weeks. Tumors were removed, weighed and measured. Inhibition of p300 decreases the tumor burden (A and B) and tumor invasion into the abdominal cavity (C and D). For the analysis of tumor burden, both tumor weight and tumor volume were analyzed; $p < 0.05$, Mann Whitney U-test.

in 4% fetal bovine serum in PBS 1×. They were then incubated overnight at 4 °C with primary antibodies, followed by 30 min incubation with diluted biotinylated secondary antibody and then 30 min incubation with Vectastain ABC reagent (Vector Laboratories Inc.). Diaminobenzidine/H_2O_2 were used as substrates for the immunoperoxidase reaction. They were lightly counterstained with Harris hematoxylin (Zymed Laboratories), dehydrated through graded ethanol and xylene, mounted with Permount (Fisher Scientific) for analysis by bright field microscopy, and examined under an Olympus microscope (CX31). For negative controls, the slides were subjected to the same IHC process omitting the primary antibody. Primary antibodies used were rabbit polyclonal anti-p300 (N-15 and C-20, sc-584 and 585), goat polyclonal anti-Ki-67 (M-19, sc-7846) and rabbit polyclonal anti-Bax (N-20, sc-493), from Santa Cruz Biotechnology.

2.13. Evaluation of immunohistochemical staining

All samples were evaluated and scored simultaneously by a pathologist (JA) and two graduate students (NG and DS), all of them blinded to sample information. Immunostained sections were scored semiquantitatively based upon the proportion of tumor cells stained and the staining intensity, using the Immuno-Reactive-Score (IRS) system (combining positive cell ratio and staining intensity) as suggested by Remmele and Stegner (1987). Staining intensity for p300 was graded according to the following criteria: 0 (−, no staining); 1 (+, weak staining = light yellow); 2 (++, moderate staining = yellow brown) and 3 (+++, strong staining = brown). IRS is the product of staining intensity and the percentage of positively stained cells (graded between 0 and 4, being 1 = <25%, 2 = 25–50%; 3 = 51–75%, and 4 = >75%, respectively). Bax and Ki-67 expressions were evaluated as previously described (Facchinetti et al., 2010). The IRS was calculated as the product of the staining intensity (graded as: 0 = no, 1 = weak, 2 = moderate and 3 = strong staining) by the percentage of positively stained cells (0 = less than 10% of stained cells, 1 = 11–50% of stained cells, 2 = 51–80% of stained cells and 3 = more than 81% of stained cells). The mean IRSs for p300, Bax and Ki 67 in 10 randomly chosen fields of the sample (400× magnification) were determined. To semi-quantify p300 subcellular localization, the total percentage of positive cytoplasm and/or nucleus for p300 was assessed. The samples showing cytoplasmic, and those showing nuclear and cytoplasmic p300 staining were grouped under "cytoplasmic staining". The samples with p300 exclusively nuclear were described as "only nuclear staining". The mean

Please cite this article as: Fermento, M.E., et al., Inhibition of p300 suppresses growth of breast cancer. Role of p300 subcellular localization, Exp. Mol. Pathol. (2014), http://dx.doi.org/10.1016/j.yexmp.2014.09.019

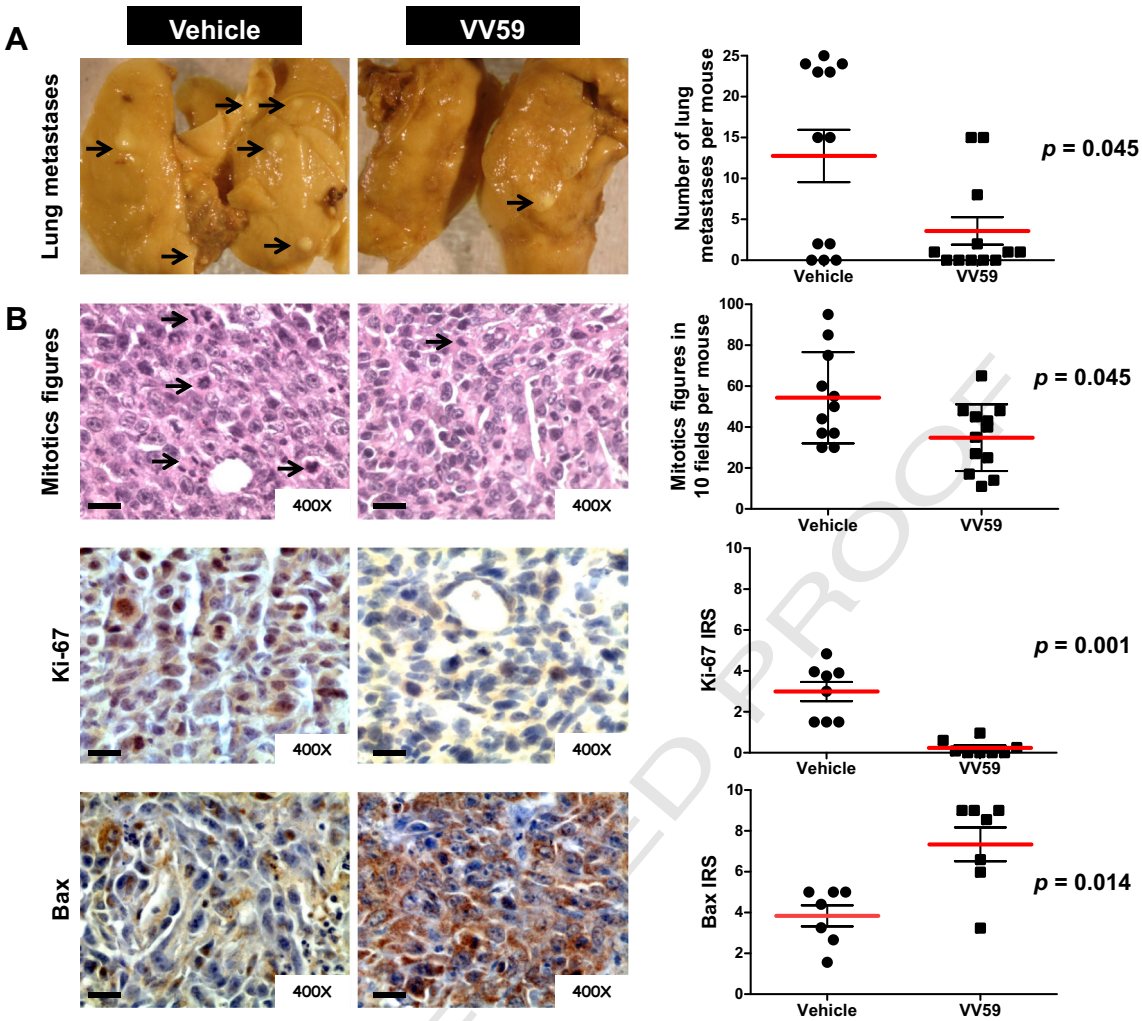

Fig. 6. p300 inhibition decreases lung metastases, mitotic index, and Ki-67 and increases Bax in subcutaneous primary tumors. A. Representative pictures of the metastases observed in the lungs from mice treated with vehicle and VV59 and their quantification. B. Subcutaneous primary tumor tissues: representative micrographs of H&E showing mitotic figures and immunohistochemical staining showing Ki-67 and Bax and their quantification; $p < 0.05$, Mann Whitney U-test; *scale bars* represent 40 μm.

percentage for p300 localization in 10 randomly chosen fields of the sample (400× magnification) was determined.

2.14. Statistical analysis

Experiments were performed in triplicate and results were recorded. All data were entered into a standardized electronic spreadsheet (Excel for Microsoft Windows). The GraphPad Prism software package, version 5.00 was used for collection, processing and statistical analysis of all data. In cell lines and animal model experiments, data were presented as means ± standard deviation (SD); Student's t test, one-way analysis of variance and non-parametric tests were used to analyze the significance between groups. Statistical significance was determined at $p < 0.05$ level. Analysis of cell count and migration assays was performed with two-way Anova. Comparison of the number of lung metastases among different groups was made by the non-parametrical Mann–Whitney U test. In human biopsy studies, statistical analysis was performed using the non-parametrical Mann–Whitney U test. χ^2 test was performed to analyze possible associations between p300 expression and clinical parameters. The cumulative survival time was computed using the Kaplan–Meier method and compared by the log-rank test. Multivariate analyses were based on the Cox proportional hazards regression model. All *p*-values resulted from two-sided statistical tests and $p < 0.05$ was considered to be significant.

3. Results

3.1. Inhibition of p300 decreases cell number of LM3 cell line

Lys-CoA and H3-CoA-20 are synthetic HAT inhibitors that are specific for p300 and for PCAF, respectively. However, these agents are not easily able to permeate cells (Cebrat et al., 2003; Lau et al., 2000). Instead, derivatives of anacardic acid were shown to be potent inhibitors of p300 and permeate cells (Eliseeva et al., 2007). Moreover, it has been reported that a cell-permeable natural compound, curcumin, possesses HAT inhibitory activity with specificity for p300/CBP (Balasubramanyam et al., 2004). Therefore, in this work we have used two synthetic inhibitors of p300, VV56 and VV59, which are derivatives of anacardic acid, for most assays. These inhibitors have been demonstrated to potently inhibit the proliferation of several cancer cell lines and to suppress p300 activity in MCF7 breast cancer cell line (Eliseeva et al., 2007). Curcumin was further used for in vivo animal studies.

To investigate the role of p300 on cell viability, LM3 cells were treated with the synthetic inhibitors VV59 and VV56 at different times of incubation (12, 24, 48, 72 h) and different concentrations (25, 50, 75 and 100 μM) and both manual counting and WST-1 assays were performed. A decrease in cell count was observed from 50 μM and 12 h onwards for VV56 and VV59, compared to vehicle-treated cells (Fig. 1A and B). Furthermore, a decrease in cell count was observed with 25 μM from 48 h

Please cite this article as: Fermento, M.E., et al., Inhibition of p300 suppresses growth of breast cancer. Role of p300 subcellular localization, Exp. Mol. Pathol. (2014), http://dx.doi.org/10.1016/j.yexmp.2014.09.019

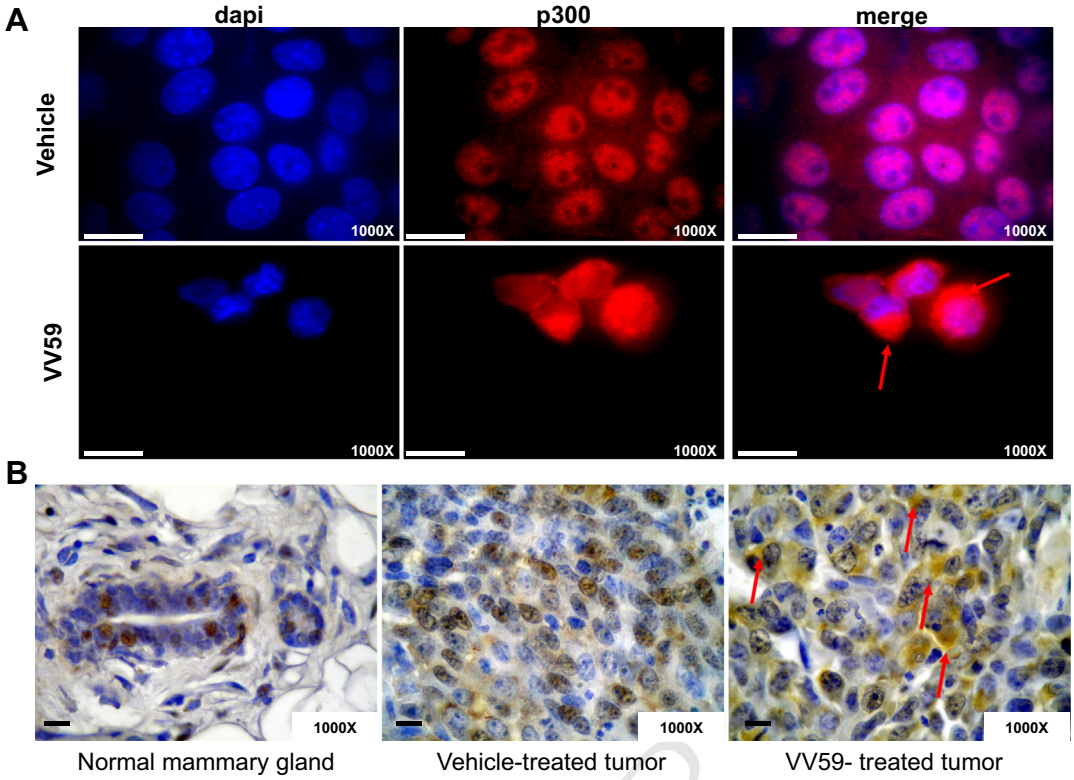

Fig. 7. p300 inhibition induces its cytoplasmic localization. A. IF showing the expression of p300 in LM3 cell line. Inhibition of p300 with VV59 increases its cytoplasmic localization (red arrows), *scale bars* represent 20 μm. B. IHC showing staining of p300 in normal mammary gland and tumors of the syngeneic animal model of LM3. Inhibition of p300 increases its cytoplasmic localization (red arrows), *scale bars* represent 20 μm. (For interpretation of the references to color in this figure legend, the reader is referred to the web version of this article.)

onwards for VV59, compared to vehicle-treated cells (Fig. 1B). As a greater inhibitory effect was observed with VV59 we decided to use this inhibitor for further viability studies.

3.2. Inhibition of p300 induces apoptosis in LM3 cells

In order to investigate the mechanisms responsible for the decrease in LM3 cell viability in, we performed PI staining followed by flow cytometry analysis. After 24 h of VV59 (50 μM) treatment, the percentage of cells in the G0/G1 population decreased to 43.92%, compared to 62.06% in the vehicle-treated cells and the proportion of cells in the sub-G0 population increased to 13.1% compared to 3.57% in the controls (Fig. 2A). In order to corroborate if this increase in subG0 population was due to an induction of apoptosis, annexin V (AV) staining was performed after 18 h of VV59 (50 μM) incubation. The apoptotic population (AV +/ PI −) increased from 4.57% in the vehicle-treated cells to 21.15% in the VV59-treated cells (Fig. 2B).

We further analyzed the expression of proteins involved in this process. We found that p21, p53 and Bax were up-regulated and pBad was down-regulated when the cells were treated with the inhibitor whereas levels of cyclins D1 and E and p27 remained constant (Fig. 2C). Altogether these results indicate that p300 inhibition results in an induction of the apoptotic process.

3.3. Inhibition of p300 decreases cell migration of LM3 cell line

Since there is evidence that p300 is important for tumor cell growth and migration (Zhou et al., 2014), we evaluated whether p300 holds an effect on cell migration by performing a wound healing assay. Confluent monolayers of LM3 cells treated with VV56 (12.5 μM), VV59 (12.5 μM) or vehicle for 24 h were wounded and observed by optical microscopy every 4 h over a period of 24 h. LM3 cells treated with vehicle migrated and closed the wound within 24 h (wound uncovered area 5.18%) whereas those cells treated with VV56 or VV59 presented a significant uncovered area of the wound in the same period of time (50.6% and 75% respectively, $p < 0.001$; Fig. 3A). As a stronger effect on cell migration was observed with VV59 we decided to use this inhibitor for invasion studies using Matrigel chambers. VV59 treatment significantly reduced the invasiveness of LM3 when compared with vehicle treatment (mean ± SD of vehicle treatment = 65.36 ± 1.89; mean ± SD of VV59 treatment = 45.85 ± 2.55, $p < 0.0001$; Fig. 3B).

3.4. Inhibition of p300 impairs lamellipodium formation in LM3 cells

Initiation of migration in epithelial cells is characterized by the rapid reorganization of the actin cytoskeleton to the cell edge, resulting in the protrusion of a leading lamellipodium at the advancing front of the cells. Having seen the effect of VV59 on migration and invasion in LM3 cell line, we analyzed if p300 inhibition affected the formation of lamellipodium by staining F-actin with phalloidin-TRITC. The number of lamellipodia was strongly reduced in LM3 cell line when it was treated with VV59 (12.5 μM, 12 h; $p = 0.003$) as observed by immunofluorescence (Fig. 4A and B) and confocal microscopy (Fig. 4C). In addition, a change in the morphology of the cells was observed (Fig. 4D). Thus, the decreased migration of VV59-treated cells in the wound assay may be the result of a reduced ability of cells to extend membrane mobile structures and to reorganize their cellular cytoskeleton when p300 is inhibited.

3.5. Inhibition of p300 reduces tumor burden, lung metastases and tumor invasion into the abdominal cavity in a murine model of breast cancer

In order to gain insight into the significance of p300 in BC and with the aim at evaluating if inhibition of p300 exerts an effect in vivo, a syngeneic animal model of subcutaneous injection of LM3 cells was

Please cite this article as: Fermento, M.E., et al., Inhibition of p300 suppresses growth of breast cancer. Role of p300 subcellular localization, Exp. Mol. Pathol. (2014), http://dx.doi.org/10.1016/j.yexmp.2014.09.019

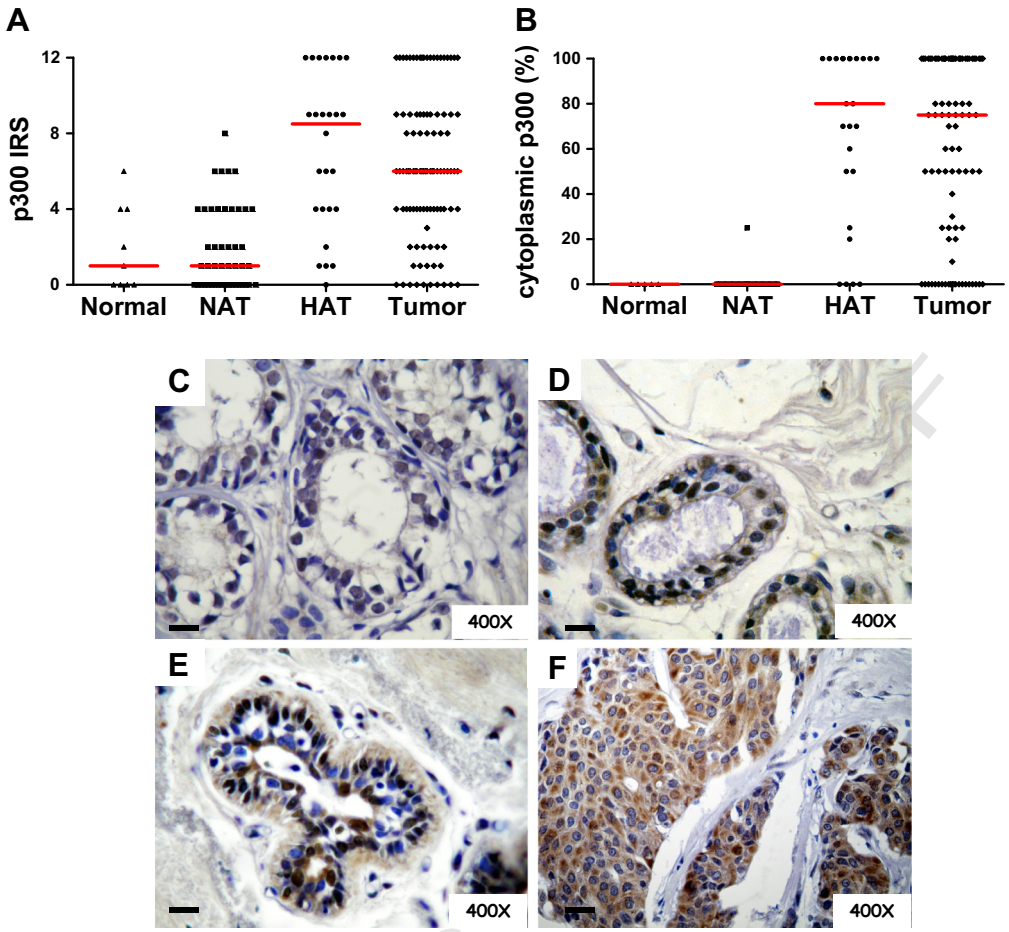

Fig. 8. p300 is overexpressed and localized to cytoplasm in human mammary tumor tissues. A. Immunohistochemical evaluation of total p300 expression in non-malignant mammary glands (Normal), normal adjacent tissues (NAT), hyperplastic tissues adjacent to the tumor tissues (HAT) and tumor tissues (Tumor). B. Immunohistochemical evaluation of cytoplasmic p300 expression in non-malignant mammary glands (Normal), normal adjacent tissues (NAT), hyperplastic tissues adjacent to the tumor tissues (HAT) and tumor tissues (Tumor). C–F: photomicrographs showing the protein expression patterns of p300 in non-malignant mammary gland (C), NAT (D), HAT (E) and tumor (F) tissues, *scale bars* represent 40 μm.

performed. As a stronger effect on cell migration and proliferation was observed with VV59, we decided to use this inhibitor for in vivo studies. In addition, we also used curcumin that has been widely used to inhibit p300. Treatment of animals with p300 inhibitors (curcumin and VV59) was performed as described in the Materials and methods section. As shown in Fig. 5A the tumor weight and volume were significantly decreased in those animals treated with curcumin compared to the vehicle-treated mice (1.52 ± 0.73 g versus 3.46 ± 1.15 g, $p = 0.016$ and 996 ± 670 mm^3 versus 2900 ± 1130 mm^3, $p = 0.048$). Similarly, treatment of animals with VV59 produced a decrease in tumor weight and volume compared to treatment with vehicle (1.23 ± 0.81 g versus 2.24 ± 1.17 g, $p = 0.032$ and 707 ± 546 mm^3 versus 1807 mm^3 ± 1111, $p = 0.010$) as shown in Fig. 5B. Interestingly, curcumin and VV59 treatment impaired the invasion through the abdominal muscle wall. Thus, 17% of the animals treated with curcumin versus 83% of the animals treated with vehicle invaded through the abdominal muscle wall. Similarly, 25% of the animals treated with VV59 versus 75% of the animals treated with vehicle invaded through the abdominal muscle wall (Fig. 5C and D). The LM3 syngeneic murine model of breast cancer produces lung metastases (Urtreger et al., 1997) and therefore it is a good model to study the effect of p300 inhibition on this process. Interestingly, and in concordance with the previously observed effect on LM3 cell migration and invasion, we found a lower number of lung metastases per animal in VV59-treated mice than in the vehicle-treated mice (mean 3.58 versus 12.75 respectively; $p = 0.045$; Fig. 6A).

Since a reduction in tumor burden was observed with VV59 treatment we aim at studying whether apoptosis and/or proliferation processes were affected in animal primary tumors. To study proliferation we examined the number of mitotic figures in H&E-stained tumor slides and Ki-67 expression by immunohistochemistry and to examine apoptosis we evaluated expression of Bax by immunohistochemistry. In tumors of mice treated with VV59, we observed fewer mitotic figures compared to vehicle administration (mean 34.83 versus mean 54.36 mitotic figures per ten fields, respectively, $p = 0.045$, Fig. 6B). Furthermore, the expression of Ki-67 in tumors decreased in VV59-treated mice compared to vehicle-treated animals (mean IRS = 0.24 versus 2.99, respectively; $p = 0.001$, Fig. 6B). On the contrary, the expression of Bax in tumors increased in VV59-treated mice compared to vehicle-treated mice (mean IRS = 7.39 versus 3.84, respectively; $p = 0.014$ Fig. 6B). These results suggest that p300 inhibition in vivo impairs tumor growth by reducing proliferation and inducing apoptosis.

3.6. Inhibition of p300 induces an increase in p300 cytoplasmic localization in LM3 cell line and in tumors of the LM3 syngeneic animal model

Since there is evidence that p300 localizes to the cytoplasm both to be degraded in proteasomes (J. Chen et al., 2007; Y. Chen et al., 2007) Q8 and to modulate p53 tumor suppressor protein levels (Shi et al., 2009), we studied p300 subcellular localization by IF in the LM3 cell

Please cite this article as: Fermento, M.E., et al., Inhibition of p300 suppresses growth of breast cancer. Role of p300 subcellular localization, Exp. Mol. Pathol. (2014), http://dx.doi.org/10.1016/j.yexmp.2014.09.019

Table 1
Clinical and pathological features of the breast cancer population in relation to p300 expression.

Clinical classification	Total	Immunostaining results (no. of patients (%))		p-Value[a]
		p300 expression		
		+	−	
Age at surgery (years)				
<49	29	27 (93.1)	2 (6.9)	0.049
50–60	28	27 (96.4)	1 (3.6)	
>61	26	20 (76.9)	6 (23.1)	
Stage				
I	26	23 (88.5)	3 (11.5)	0.081
II	30	29 (96.7)	1 (3.3)	
III	21	16 (76.2)	5 (23.8)	
NA[b]	6	–	–	
T (TNM)				
T1 (<2 cm)	37	36 (97.3)	1 (2.7)	0.007
T2 (>2 a < =5 cm)	31	29 (93.5)	2 (6.45)	
T3 (>5 cm)	13	9 (69.2)	4 (30.8)	
NA	2	–	–	
N-regional lymph node				
N (−)	46	42 (91.3)	4 (8.7)	0.293
N (+)	30	25 (83.3)	5 (16.7)	
NA	7	–	–	
Recurrence				
Absent	38	37 (97.4)	1 (2.6)	0.048
Present	24	20 (83.3)	4 (16.7)	
NA	21	–	–	
Histologic grade				
I	4	4 (100)	0 (0)	0.366
II	30	25 (83.3)	5 (16.7)	
III	40	37 (92.5)	3 (7.5)	
NA	9	–	–	
Nuclear grade				
I	2	2 (100)	0 (0)	0.900
II	33	30 (90.9)	3 (9.1)	
III	25	23 (92)	2 (8)	
NA	23	–	–	
Mitotic index				
I	29	29 (100)	0 (0)	0.115
II	13	11 (84.6)	2 (15.4)	
III	10	9 (90)	1 (10)	
NA	31	–	–	
ER				
Positive	24	20 (83.3)	4 (16.7)	0.106
Negative	55	52 (94.5)	3 (5.5)	
NA	4	–	–	
PR				
Positive	20	18 (90)	2 (10)	0.819
Negative	60	55 (91.7)	5 (8.3)	
NA	3	–	–	
Her2				
Positive	21	19 (90.5)	2 (9.5)	0.550
Negative	53	50 (94.3)	3 (5.7)	
NA	9	–	–	

[a] Chi-square test, difference of $p < 0.05$ was considered to be significant.
[b] NA: not available.

line and by IHC in tumors of the syngeneic murine model. When we treated LM3 cells with VV59, the expression of p300 increased compared to vehicle treatment (median IRS: 12 versus IRS: 8, respectively; $p < 0.001$; data not shown). Regarding p300 subcellular localization, nuclear localization and cytoplasmic localization were observed in cells treated with VV59 while only nuclear p300 localization was observed in cells treated with vehicle (Fig. 7A). Furthermore, in the LM3 murine model of BC, p300 expression was mostly nuclear in vehicle-treated tumors and both cytoplasmic and nuclear in VV59-treated tumors (Fig. 7B).

3.7. Human breast cancer tumors present an unusual cytoplasmic localization of p300

In order to investigate the role of p300 in human breast cancer, we studied p300 expression in human tumors and its correlation with clinic-pathological data.

For this purpose we performed immunohistochemistry in a series of paraffin-embedded tissue biopsies comparing the p300 expression in non-malignant mammary glands (normal), in areas with normal histology adjacent to the tumor tissues (normal adjacent tissues, NAT), in hyperplastic tissues adjacent to the tumor tissues (HAT) and in tumor tissues (tumor).

Interestingly, tumor specimens showed higher prevalence of expression (90%, 91/101) than normal mammary glands (55%, 5/9; $p = 0.029$). In addition, tumor specimens also showed higher prevalence of p300 expression than NAT. In NAT, 62.5% (30/48) of the samples showed p300 expression (data not shown).

Moreover, the levels of p300 in tumor tissues were significantly higher than in non-malignant mammary glands (median IRS 6.00 versus median IRS 1.00, respectively; $p = 0.0012$; Fig. 8A). The levels of p300 in tumor tissues were also higher than in NAT (median IRS 6.00 versus 1.00; $p < 0.0001$; Fig. 8A). Interestingly, the levels of p300 were already increased in HAT, not being significantly different to those of tumor tissues (Fig. 8A). Representative pictures from selected additional human samples can be seen in Supplementary Fig. 1.

Regarding the subcellular localization, p300 was exclusively nuclear in normal tissues when present, as expected (Fig. 8B and C). Surprisingly an unusual cytoplasmic localization for p300 was observed in tumor tissues (Fig. 8B and F). p300 was cytoplasmic in 76.9% (70/91) and only nuclear in 23.1% (21/91) of the tumor samples. The extent of p300 cytoplasmic expression was also evaluated (Fig. 8B). The median of the percentage of cells with p300 cytoplasmic localization in tumors (Fig. 8B and F) was 75% compared with 0% in normal mammary glands (Fig. 8B and C) and 0% in NAT ($p < 0.0001$; Fig. 8B and D). Interestingly, cytoplasmic localization of p300 was already detected in HAT (Fig. 8B and E) not being significantly different to those of tumor tissues (Fig. 8B and F).

In summary, these results show higher expression of p300 in human mammary tumors compared to normal mammary tissues and an unusual cytoplasmic localization exclusively in tumor tissues.

3.8. Cytoplasmic localization of p300 is associated with increased overall survival time of BC patients

We further studied the correlation between p300 expression and subcellular localization with several clinical and pathological parameters relevant for BC prognosis such as age at surgery, stage, tumor size, lymph node status, tumor recurrence, histological grade, nuclear grade, mitotic index and estrogen receptor (ER), progesterone receptor (PR) and human epidermal growth factor receptor 2 (Her2) statuses. This analysis revealed a significant correlation between p300 positive expression and age ($p = 0.049$), tumor size ($p = 0.0071$) and tumor recurrence ($p = 0.048$, Table 1). Also, we found a significant correlation between p300 cytoplasmic expression and tumor size ($p = 0.026$; Fig. 9A, upper graph) and tumor recurrence ($p = 0.027$; Fig. 9A, lower graph and Table 2).

Since features that are known to have a prognostic influence may covariate, the correlation between p300 expression and these features was further examined in multivariate analysis. We modeled not only the relationship between the survival rate and time, but also the possible relationship between the different variables recorded for each subject. The variables included in the model were: p300, age at surgery, alcohol consumption, smoking habit, clinical stage, lymph node metastasis, family

Please cite this article as: Fermento, M.E., et al., Inhibition of p300 suppresses growth of breast cancer. Role of p300 subcellular localization, Exp. Mol. Pathol. (2014), http://dx.doi.org/10.1016/j.yexmp.2014.09.019

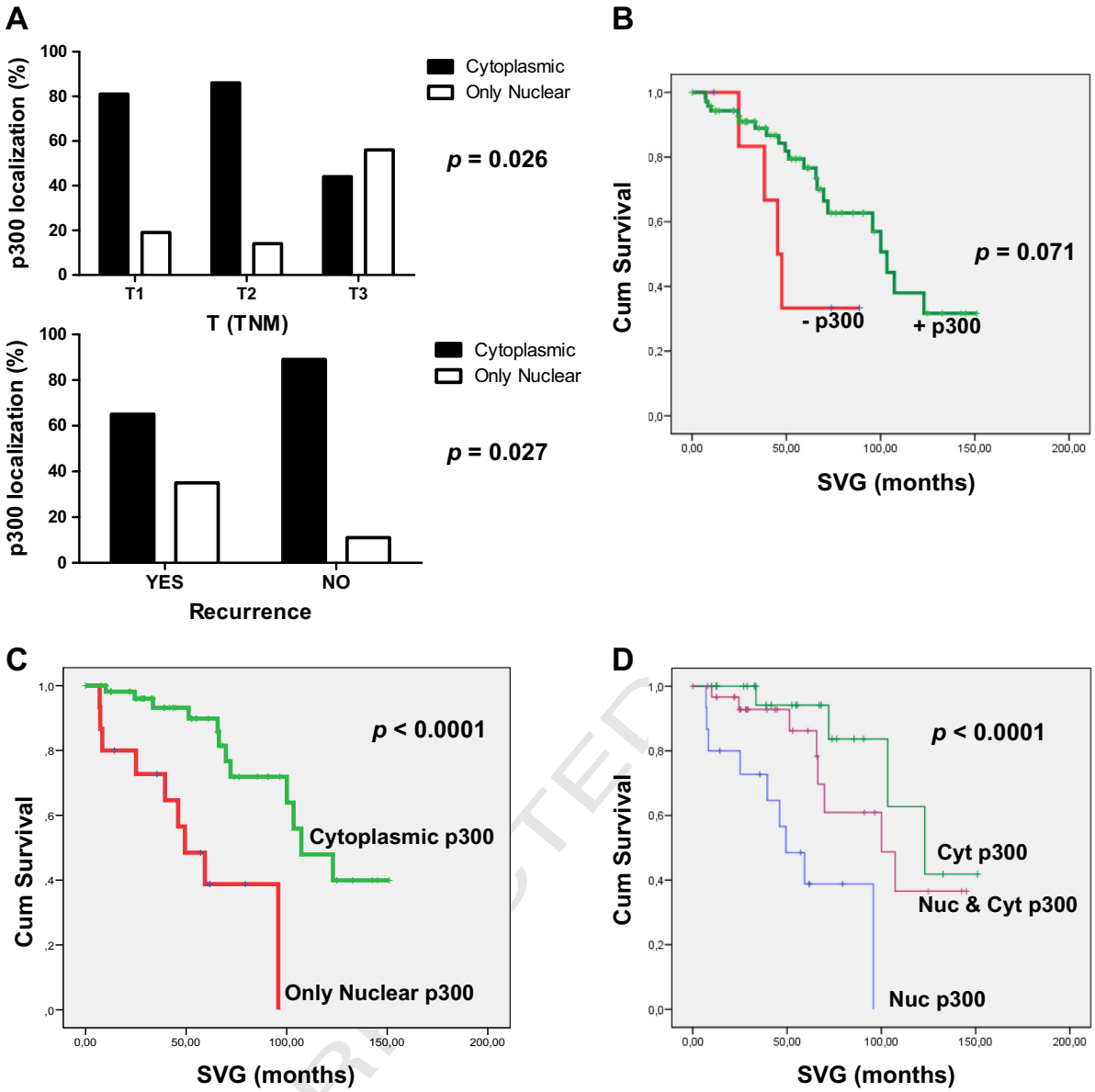

Fig. 9. Cytoplasmic localization of p300 is associated with increased overall survival time of BC patients. A. Correlation of p300 cytoplasmic localization with the tumor size (T) (upper graph) or disease recurrence (bottom graph). B. Kaplan–Meier survival curves for BC patients stratified according to absence or presence of p300 expression (log-rank test). C. Kaplan–Meier survival curves for BC patients stratified according to cytoplasmic p300 or only nuclear p300 localization (log-rank test). D. Kaplan–Meier survival curves for BC patients stratified according to cytoplasmic p300 (Cyt), nuclear and cytoplasmic p300 (Nuc & Cyt) or only nuclear p300 (Nuc) localization.

history, neoadjuvant therapy, surgery, hormone therapy, radiotherapy, ER status, PR status, Her2 status and overall survival (SVG) status. The variables that intervene in the equation are p300, smoking habit, and hormone; hence they are influential variables on survival (Table 3).

Then, we estimated the survival function (for overall survival) using the Kaplan–Meier estimator, taking the p300 variable as factor. Unexpectedly, we observed no significant differences between the survival distributions of patients with negative expression (n = 7) and positive expression (n = 72) of p300 ($p = 0.071$, Log Rank (Mantel–Cox) test, Fig. 9B).

We further studied if p300 subcellular localization was correlated with patient survival. Indeed, we found that localization of p300 and cigarettes are influential variables on survival (Table 4) and we observed that patients whose tumors present cytoplasmic p300 (median 107.3 months) have longer survival time than those whose tumors present exclusively nuclear expression of p300 (median 49.4 months; $p < 0.0001$, Log Rank (Mantel–Cox), Fig. 9C).

Since some tumors present exclusively cytoplasmic localization while others present both cytoplasmic and nuclear expressions we therefore distributed the patients in three groups: only nuclear p300-, only cytoplasmic p300- and both nuclear and cytoplasmic p300-tumors, and studied the association with patient survival. Patients whose tumors presented exclusively cytoplasmic p300 (median 123 months) had longer survival time than those presenting cytoplasmic and nuclear p300 (median 100 months) and the latter had longer survival time than those presenting only nuclear (median 49.4 months; $p < 0.0001$ Log Rank (Mantel–Cox), Fig. 9D).

4. Discussion

In this study we demonstrated that the inhibition of the acetyltransferase activity of p300 induces apoptosis and reduces cellular invasion in LM3 murine mammary carcinoma cell line. Furthermore, p300

Please cite this article as: Fermento, M.E., et al., Inhibition of p300 suppresses growth of breast cancer. Role of p300 subcellular localization, Exp. Mol. Pathol. (2014), http://dx.doi.org/10.1016/j.yexmp.2014.09.019

Table 2
Clinicopathological features of the breast cancer population in relation to p300 localization.

Clinical classification	Total	Immunostaining results (no. of patients (%))		p-Value[a]
		p300 cytoplasmic staining		
		+	−	
Age at surgery (years)				
<49	27	22 (81.5)	5 (18.5)	0.643
50–60	27	20 (74.1)	7 (25.9)	
>61	20	14 (70.0)	6 (30.0)	
Stage				
I	23	20 (87.0)	3 (13.0)	0.544
II	29	22 (75.9)	7 (24.1)	
III	16	12 (75.0)	4 (25.0)	
NA[b]	6	–	–	
T (TNM)				
T1 (<2 cm)	36	29 (80.6)	7 (19.4)	0.026
T2 (>2 a < =5 cm)	29	25 (86.20)	4 (13.8)	
T3 (>5 cm)	9	4 (44.4)	5 (55.6)	
N-regional lymph node				
N (−)	42	34 (81.0)	8 (19.0)	0.629
N (+)	25	19 (76)	6 (24)	
NA	7	–	–	
Recurrence				
Absent	37	33 (89.2)	4 (10.8)	0.027
Present	20	13 (65.0)	7 (35.0)	
NA	17	–	–	
Histologic grade				
I	4	2 (50)	2 (50)	0.265
II	25	19 (76.0)	6 (24.0)	
III	37	31 (83.8)	6 (16.2)	
NA	8	–	–	
Nuclear grade				
I	2	2 (100)	0 (0)	0.648
II	30	24 (80.0)	6 (20.0)	
III	23	20 (87.0)	3 (13.0)	
NA	19	–	–	
Mitotic index				
I	29	23 (79.3)	6 (20.7)	0.810
II	11	9 (81.8)	2 (18.2)	
III	9	8 (88.9)	1 (11.1)	
NA	25	–	–	
ER				
Positive	20	14 (70.0)	6 (30.0)	0.1605
Negative	52	44 (84.6)	8 (15.4)	
NA	2	–	–	
PR				
Positive	18	14 (77.8)	4 (22.2)	0.705
Negative	55	45 (81.8)	10 (18.2)	
NA	1	–	–	
Her2				
Positive	19	16 (84.2)	3 (15.8)	0.983
Negative	50	42 (84.0)	8 (16.0)	
NA	5	–	–	

[a] Chi-square test, difference of $p < 0.05$ was considered to be significant.
[b] NA: not available.

Table 3
p300 expression as influential variables on survival of patients.

Variables in the equation	B	SE	Wald	df	Sig.	Exp (B)
p300 expression	−2.971	1.019	8.501	1	.004	.051
Smoking habit	−2.231	.976	5.224	1	.022	.107
Hormone therapy	−1.746	.826	4.469	1	.035	.174

Table 4
p300 localization as influential variables on survival of patients.

Variables in the equation	B	SE	Wald	df	Sig.	Exp (B)
p300 localization	−.957	.431	4.933	1	.026	.384
Smoking habit	−1.452	.683	4.522	1	.033	.234

inhibition decreases tumor burden and the number of lung metastases in a murine model of syngeneic transplantation of the LM3 cell line.

As already stated, there is evidence indicating that p300 can function both as a tumor suppressor protein and as an oncoprotein (Goodman and Smolik, 2000). Our results obtained in the LM3 murine cell line and LM3 syngeneic animal model are in agreement with those showing that p300 acts as an oncogene exerting pro-tumoral effects, such as what has been demonstrated in prostate (Debes et al., 2003), colon (Ishihama et al., 2007), leukemia (Borrow et al., 1996), and lung (Karamouzis et al., 2007) cancers. Furthermore, our results are also in agreement with previous reports demonstrating that inhibitors of p300 acetyl-transferase activity are potent anticancer agents (Yang et al., 2013) and that inhibition of p300 is an effective strategy for treating triple negative BC (Liao et al., 2012).

In regard to p300 expression and the role it plays in human cancer it has been described that overexpression of this protein in human colon adenocarcinoma was indicative of poor prognosis (Ishihama et al., 2007). In addition, p300 expression was found to be related to tumor proliferation and to be predictive for progression of disease after surgery in prostate cancer (Debes et al., 2003). Similarly, in both hepatocellular carcinoma and esophageal squamous cell carcinoma high expression of the transcriptional coactivator p300 was correlated with aggressive features and poor prognosis (M. Li et al., 2011; Y. Li et al., 2011). All these reports show a pro-tumoral role for p300 in human cancer.

In relation to the role of p300 in human breast cancer tissues conflicting results have been obtained. For example, a study showed that p300 mRNA levels correlated with lymph node status (Kurebayashi et al., 2000). In contrast, another study has associated higher p300 protein levels with lower tumor grade and type (Green et al., 2008). In addition it has been demonstrated that p300 protein levels did not correlate with tumor grade (Vleugel et al., 2006) or with nodal positivity (Hudelist et al., 2003).

Our studies show that p300 is overexpressed in human mammary tumor tissues when compared to both non-malignant mammary tissues and histologically normal adjacent tissues in accordance to what was reported for human breast carcinomas (Hudelist et al., 2003; Xiao et al., 2011). Interestingly, p300 expression correlated with lower tumor size and absence of recurrence, in agreement with the results obtained by Green et al. (2008), although it was not associated with patient survival time. This absence of correlation between p300 expression and patient survival is surprising in light of our results in LM3 breast cancer cell line and LM3 syngeneic animal model described above. In this regard, our observation about the correlation between p300 cytoplasmic localization and longer patient survival time is interesting. This correlation seems not to agree with a previous report showing that high expression of p300 in human BC correlates with tumor recurrence and predicts poor prognosis of patients (Xiao et al., 2011). However, it is interesting to note that the authors say that "yellowish brown granules could also be seen in the cytoplasm (Fig. 2)", although studies of correlation between cytoplasmic localization and patient survival time were not performed in this work. Furthermore, this study was performed in tissue microarrays and it is known that due to size of the cores in the microarrays they are not representative of the whole tumor. In addition Hudelist et al. (2003) stated that p300 "was usually also detectable in the cytoplasm" in breast cancer. Cytoplasmic p300 was also observed in non-small cell lung cancer (Gao et al., 2014) and in melanoma (Bhandaru et al., 2014; Rotte et al., 2013).

Please cite this article as: Fermento, M.E., et al., Inhibition of p300 suppresses growth of breast cancer. Role of p300 subcellular localization, Exp. Mol. Pathol. (2014), http://dx.doi.org/10.1016/j.yexmp.2014.09.019

Importantly, it has been shown that p300 distribution between the nucleus and cytoplasm may be modulated and that its cytoplasmic localization may be associated with a specific biological activity. Thus, Q10 J. Chen et al. (2007) and Y. Chen et al. (2007) reported a ubiquitin-dependent distribution of p300 in cytoplasmic inclusion bodies and showed evidence that cellular trafficking and redistribution regulate the availability and activity of this cofactor. Importantly, Shi et al. (2009) demonstrated the presence of cytoplasmic p300 in human osteosarcoma cells (U2OS), and assigned a role for this cytoplasmic p300 in p53 degradation. Our data strongly corroborates p300 cytoplasmic localization in breast cancer. Importantly, our study in human primary breast carcinoma specimens demonstrates that p300 is mainly nuclear in adjacent areas to the tumor whereas it is localized both in the cytoplasm and nucleus in malignant epithelial cells. Also, this study is the first to demonstrate that cytoplasmic localization of p300 is associated with improved patient survival and reduced tumor size. Interestingly, we observe p300 cytoplasmic location following pharmacological inhibition of p300 in both LM3 murine cell line and LM3 animal model. The physical removal of p300 from the nucleus might serve as a mechanism to modulate the function of this coactivator, by limiting its interaction with sequence-specific transcription factors, and to regulate gene activation. Furthermore, cytoplasmic p300 may also be playing a role in modulating HDAC6 activity since a recent report presented evidence of a role of cytoplasmic p300 in attenuating HDAC6 deacetylase activity and thus influencing tubulin acetylation and motility (Han et al., 2009). Finally, p300 mutations that have been reported in breast cancer (Gayther et al., 2000) might also play a role in affecting its cellular localization.

5. Conclusions

We provided evidence that p300 is involved in BC progression by promoting cellular invasion and cellular survival, as demonstrated in a murine breast adenocarcinoma cell line and animal model. Altogether, these results support the hypothesis that, at least in breast carcinomas, p300 acts as an oncogene. Furthermore, we demonstrated that cytoplasmic p300 is overexpressed in human BC and that this cytoplasmic localization is associated with a reduced tumor size, lower recurrence rates and an increase in the overall survival time of patients. Altogether these results suggest that it is possible that a cytoplasmic localization of p300 precludes its pro-tumoral effects and thereby promote survival rate of patients, thus explaining the dual role observed for this co-factor in cancer.

Supplementary data to this article can be found online at http://dx.doi.org/10.1016/j.yexmp.2014.09.019.

Conflict of interest statement

The authors declare that there are no conflicts of interest.

Acknowledgments

This work was supported by the Agencia Nacional de Promoción Q11 Científica y Tecnológica (ANPCyT), the Consejo Nacional de Q13 Q12 Investigaciones Científicas y Técnicas (CONICET) and by Universidad Q14 Nacional del Sur, Bahía Blanca, Buenos Aires, Argentina. María E. Fermento, Norberto A. Gandini, Débora G. Salomón and María J Ferronato are recipients of a fellowship from CONICET. We are very grateful to Dr Elisa Bal de Kier Joffe (Instituto Roffo, Buenos Aires, Argentina) for providing the LM3 cells. M. J. thanks the Deutsche Forschungsgemeinschaft (DFG, Ju295/9-2, within SPP1463) for funding.

References

Avantaggiati, M.L., Ogryzko, V., Gardner, K., Giordano, A., Levine, A.S., Kelly, K., 1997. Recruitment of p300/CBP in p53-dependent signal pathways. Cell 89 (7), 1175–1184.

Balasubramanyam, K., Varier, R.A., Altaf, M., Swaminathan, V., Siddappa, N.B., Ranga, U., Kundu, T.K., 2004. Curcumin, a novel p300/CREB-binding protein-specific inhibitor of acetyltransferase, represses the acetylation of histone/nonhistone proteins and histone acetyltransferase-dependent chromatin transcription. J. Biol. Chem. 279 (49), 51163–51171.

Bannister, A.J., Kouzarides, T., 1996. The CBP co-activator is a histone acetyltransferase. Nature 384, 641–643.

Bannister, A.J., Miska, E.A., 2000. Regulation of gene expression by transcription factor acetylation. Cell. Mol. Life Sci. 57 (8–9), 1184–1192.

Bhandaru, M., Ardekani, G.S., Zhang, G., Martinka, M., McElwee, K.J., Li, G., Rotte, A., 2014. A combination of p300 and Braf expression in the diagnosis and prognosis of melanoma. BMC Cancer 14, 398–409.

Borrow, J., Stanton, V.P., Andresen, J.M., Becher, R., Behm, F.G., Chaganti, R.S.K., Civin, C.I., Disteche, C., Dubé, I., Frischauf, A.M., Horsman, D., Mitelman, F., Volinia, S., Watmore, A.E., Housman, D.E., 1996. The translocation t (8;16)(p11;p13) of acute myeloid leukaemia fuses a putative acetyltransferase to the CREB-binding protein. Nat. Genet. 14, 33–41.

Bruzzone, A., Vanzulli, S.I., Soldati, R., Giulianelli, S., Lanari, C., Luthy, I.A., 2009. Novel human breast cancer cell lines IBH-4, IBH-6, and IBH-7 growing in nude mice. J. Cell. Physiol. 219, 477–484.

Cebrat, M., Kim, C.M., Thompson, P.R., Daugherty, M., Cole, P.A., 2003. Synthesis and analysis of potential prodrugs of coenzyme A analogues for the inhibition of the histone acetyltransferase p300. Bioorg. Med. Chem. 11, 3307–3313.

Chan, H.M., La Thangue, N.B., 2001. p300/CBP proteins: HATs for transcriptional bridges and scaffolds. J. Cell Sci. 114 (13), 2363–2373.

Chen, J., Halappanavar, S., Th' ng, J.P., Li, Q., 2007a. Ubiquitin-dependent distribution of the transcriptional coactivator p300 in cytoplasmic inclusion bodies. Epigenetics 2 (2), 92–99.

Chen, Y., Shu, W., Chen, W., Wu, Q., Liu, H., Cui, G., 2007b. Curcumin, both histone deacetylase and p300/CBP-specific inhibitor, represses the activity of nuclear factor kappa B and Notch 1 in Raji cells. Basic Clin. Pharmacol. Toxicol. 101, 427–433.

Costanzo, A., Merlo, P., Pediconi, N., Fulco, M., Sartorelli, V., Cole, P.A., Fontemaggi, G., Fanciulli, M., Schiltz, L., Blandino, G., Balsano, C., Levrero, M., 2002. DNA damage-dependent acetylation of p73 dictates the selective activation of apoptotic target genes. Mol. Cell 9 (1), 175–186.

de Matos, D.C., de Ribeiro, L.C.A., Tansini, A., Ferreira, L.S., Placeres, M.C.P., Colombo, L.L., Carlos, I.Z., 2012. Immunological response in mice bearing LM3 breast tumor undergoing pulchellin treatment. BMC Complement. Altern. Med. 12 (107), 2–6.

Debes, J.D., Sebo, T.J., Lohse, C.M., Murphy, L.M., Haugen, D.A., Tindall, D.J., 2003. p300 in prostate cancer proliferation and progression. Cancer Res. 63 (22), 7638–7640.

Eliseeva, E.D., Valkov, V., Jung, M., Jung, M.O., 2007. Characterization of novel inhibitors of histone acetyltransferases. Mol. Cancer Ther. 6 (9), 2391–2398.

Facchinetti, M.M., Gandini, N.A., Fermento, M.E., Sterin-Speziale, N.B., Ji, Y., Patel, V., Gutkind, J.S., Rivadulla, M.G., Curino, A.C., 2010. The expression of sphingosine kinase-1 in head and neck carcinoma. Cells Tissues Organs 192 (5), 314–324.

Filigheddu, N., Sampietro, S., Chianale, F., Porporato, P.E., Gaggianesi, M., Gregnanin, I., Rainero, E., Ferrara, M., Perego, B., Riboni, F., Baldanzi, G., Graziani, A., Surico, N., 2011. Diacylglycerol kinase α mediates 17-β-estradiol-induced proliferation, motility, and anchorage-independent growth of Hec-1ª endometrial cancer cell line through the G protein-coupled estrogen receptor GPR30. Cell Signal. 23, 1988–1996.

Gandini, N.A., Fermento, M.E., Salomón, D.G., Blasco, J., Patel, V., Gutkind, J.S., Molinolo, A. A., Facchinetti, M.M., Curino, A.C., 2012. Nuclear localization of heme oxygenase-1 is associated with tumor progression of head and neck squamous cell carcinomas. Exp. Mol. Pathol. 93, 237–245.

Gandini, N.A., Fermento, M.E., Salomón, D.G., Obiol, D.J., Andrés, N.A., Zenklusen, J.C., Arévalo, J., Blasco, J., López Romero, A., Facchinetti, M.M., Curino, A.C., 2014. Heme oxygenase-1 expression in human gliomas and its correlation with poor prognosis in patients with astrocytoma. Tumour Biol. 35, 2803–2815.

Gao, Y., Geng, J., Hong, X., Qi, J., Teng, Y., Yang, Y., Qu, D., Chen, G., 2014. Expression of p300 and CBP is associated with poor prognosis in small cell lung cancer. Int. J. Clin. Exp. Pathol. 7 (2), 760–767.

Gayther, S.A., Batley, S.J., Linger, L., Bannister, A., Thorpe, K., Chin, S.F., Daigo, Y., Russell, P., Wilson, A., Sowter, H.M., Delhanty, J.D., Ponder, B.A., Kouzarides, T., Caldas, C., 2000. Mutations truncating the EP300 acetylase in human cancers. Nat. Genet. 24 (3), 300–303.

Giles, R.H., Peters, D.J., Breuning, M.H., 1998. Conjunction dysfunction: CBP/p300 in human disease. Trends Genet. 14 (5), 178–183.

Giordano, A., Avantaggiati, M.L., 1999. p300 and CBP: partners for life and death. J. Cell. Physiol. 181 (2), 218–230.

Goodman, R.H., Smolik, S., 2000. CBP/p300 in cell growth, transformation, and development. Genes Dev. 14 (13), 1553–1577.

Green, A.R., Burney, C., Granger, C.J., Paish, E.C., El-Sheikh, S., Rakha, E.A., Powe, D.G., Macmillan, R.D., Ellis, I.O., Stylianou, E., 2008. The prognostic significance of steroid receptor co-regulators in breast cancer: co-repressor NCOR2/SMRT is an independent indicator of poor outcome. Breast Cancer Res. Treat. 110 (3), 427–437.

Gueron, G., De Siervi, A., Ferrando, M., Salierno, M., De Luca, P., Elguero, B., Meiss, R., Navone, N., Vazquez, E., 2009. Critical role of endogenous heme oxygenase 1 as a tuner of the invasive potential of prostate cancer Cells. Mol. Cancer Res. 7 (11), 1745–1755.

Han, Y., Jeong, H.M., Jin, Y.H., Kim, Y.J., Jeong, H.G., Yeo, C.Y., Lee, K.Y., 2009. Acetylation of histone deacetylase 6 by p300 attenuates its deacetylase activity. Biochem. Biophys. Res. Commun. 383, 88–92.

Hudelist, G., Czerwenka, K., Kubista, E., Marton, E., Pischinger, K., Singer, C.F., 2003. Expression of sex steroid receptors and their co-factors in normal and malignant breast tissue: AIB1 is a carcinoma-specific co-activator. Breast Cancer Res. Treat. 78 (2), 193–204.

Huh, J.W., Kim, H.C., Kim, S.H., Park, Y.A., Cho, Y.B., Yun, S.H., Lee, W.Y., Chun, H.K., 2013. Prognostic impact of p300 expression in patients with colorectal cancer. J. Surg. Oncol. 108 (6), 374–377.

Please cite this article as: Fermento, M.E., et al., Inhibition of p300 suppresses growth of breast cancer. Role of p300 subcellular localization, Exp. Mol. Pathol. (2014), http://dx.doi.org/10.1016/j.yexmp.2014.09.019

Ishihama, K., Yamakawa, M., Semba, S., Takeda, H., Kawata, S., Kimura, S., Kimura, W., 2007. Expression of HDAC1 and CBP/p300 in human colorectal carcinomas. J. Clin. Pathol. 60 (11), 1205–1210.

Iyer, N.G., Ozdag, H., Caldas, C., 2004. p300/CBP and cancer. Oncogene 23, 4225–4231.

Jemal, A., Bray, F., Center, M.M., Ferlay, J., Ward, E., Forman, D., 2011. Global cancer statistics. CA Cancer J. Clin. 61, 69–90.

Karamouzis, M.V., Konstantinopoulos, P.A., Papavassiliou, A.G., 2007. Roles of CREB-binding protein (CBP)/p300 in respiratory epithelium tumorigenesis. Cell Res. 17, 324–332.

Kurebayashi, J., Otsuki, T., Kunisue, H., Tanaka, K., Yamamoto, S., Sonoo, H., 2000. Expression levels of estrogen receptor-alpha, estrogen receptor-beta, coactivators and corepressors in breast cancer. Clin. Cancer Res. 6, 512–518.

Lanari, C., Wargon, V., Rojas, P., Molinolo, A.A., 2012. Antiprogestins in breast cancer treatment: are we ready? Endocr. Relat. Cancer 9, 35–50.

Lau, O.D., Kundu, T.K., Soccio, R.E., Ait-Si-Ali, S., Khalil, E.M., Vassilev, A., Wolffe, A.P., Nakatani, Y., Roeder, R.G., Cole, P.A., 2000. HATs off: selective synthetic inhibitors of the histone acetyltransferases p300 and PCAF. Mol. Cell 5, 589–595.

Li, M., Luo, R.Z., Chen, J.W., Cao, Y., Lu, J.B., He, J.H., Wu, Q.L., Cai, M.Y., 2011a. High expression of transcriptional coactivator p300 correlates with aggressive features and poor prognosis of hepatocellular carcinoma. J. Transl. Med. 9 (5), 2–11.

Li, Y., Yang, H.X., Luo, R.Z., Zhang, Y., Li, M., Wang, X., Jia, W.H., 2011b. High expression of p300 has an unfavorable impact on survival in resectable esophageal squamous cell carcinoma. Ann. Thorac. Surg. 91, 1531–1538.

Liao, D., Yang, H., Luo, J., 2012. Targeting p300 for inhibiting triple negative breast cancer. Cancer Res. 72 (8), S1.

Mackeh, R., Lorin, S., Ratier, A., Mejdoubi-Charef, N., Baillet, A., Bruneel, A., Hamaï, A., Codogno, P., Poüs, C., Perdiz, D., 2014. Reactive oxygen species, AMP-activated protein kinase and the transcription cofactor p300 regulate alpha-tubulin acetyltransferase-1 (αTAT-1/MEC-17)-dependent microtubule hyperacetylation during cell stress. J. Biol. Chem. 289 (17), 11816–11828.

Ogryzko, V.V., Schiltz, R.L., Russanova, V., Howard, B.H., Nakatani, Y., 1996. The transcriptional coactivators p300 and CBP are histone acetyltransferases. Cell 87 (5), 953–959.

Petit, V., Boyer, B., Lentz, D., Turner, C.E., Thiery, J.P., Valles, A.M., 2000. Phosphorylation of tyrosine residues 31 and 118 on paxillin regulates cell migration through an association with CRK in NBT-II cells. J. Cell Biol. 148, 957–970.

Remmele, W., Stegner, H.E., 1987. Recommendation for uniform definition of an immunoreactive score (IRS) for immunohistochemical estrogen receptor detection (ER-ICA) in breast cancer tissue. Pathologe 8, 138–140.

Rotte, A., Bhandaru, M., Cheng, Y., Sjoestroem, C., Martinka, M., Li, G., 2013. Decreased expression of nuclear p300 is associated with disease progression and worse prognosis of melanoma patients. PLoS One 8 (9), 1–12.

Sebti, S., Prébois, C., Pérez-Gracia, E., Bauvy, C., Desmots, F., Pirot, N., Gongora, C., Bach, A.-S., Hubberstey, A., Palissot, V., Berchem, G., Codogno, P., Linares, L., Liaudet-Coopman, E., Pattingre, S., 2014. BAT3 modulates p300-dependent acetylation of p53 and autophagy-related protein 7 (ATG7) during autophagy. Proc. Natl. Acad. Sci. U. S. A. 111 (11), 4115–4120.

Shi, D., Pop, M.S., Kulikov, R., Love, I.M., Kung, A.L., Grossman, S.R., 2009. CBP and p300 are cytoplasmic E4 polyubiquitin ligases for p53. Proc. Natl. Acad. Sci. U. S. A. 106 (38), 16275–16280.

Sotiriou, C., Neo, S.Y., McShane, L.M., Korn, E.L., Long, P.M., Jazaeri, A., Martiat, P., Fox, S.B., Harris, A.L., Liu, E.T., 2003. Breast cancer classification and prognosis based on gene expression profiles from a population-based study. Proc. Natl. Acad. Sci. U. S. A. 100 (18), 10393–10398.

Syrjänen, S., Naud, P., Sarian, L., Derchain, S., Roteli-Martins, C., Longatto-Filho, A., Tatti, S., Branca, M., Erzen, M., Serpa-Hammes, L., Matos, J., Arlindo, F., Sakamoto-Maeda, M., Costa, S., Syrjänen, K., 2010. p300 expression is related to high-risk human papillomavirus infections and severity of cervical intraepithelial neoplasia but not to viral or disease outcomes in a longitudinal setting. Int. J. Gynecol. Pathol. 29 (2), 135–145.

Tomita, A., Towatari, M., Tsuzuki, S., Hayakawa, F., Kosugi, H., Tamai, K., Miyazaki, T., Kinoshita, T., Saito, H., 2000. c-Myb acetylation at the carboxyl-terminal conserved domain by transcriptional co-activator p300. Oncogene 19 (3), 444–451.

Urtreger, A.J., Ladeda, V.E., Puricelli, L.I., Rivelli, A., Vidal, M.C., Sacerdote de Lustig, E., de Kier, Bal, Joffé, E., 1997. Modulation of fibronectin expression and proteolytic activity associated with the invasive and metastatic phenotype in two murine mammary tumor cell lines. Int. J. Oncol. 11, 489–496.

Vleugel, M.M., Shvarts, D., van der Wall, E., van Diest, P.J., 2006. p300 and p53 levels determine activation of HIF-1 downstream targets in invasive breast cancer. Hum. Pathol. 37 (8), 1085–1092.

Xiao, X., Cai, M., Chen, J., Guan, X., Kung, H., Zeng, Y., Xie, D., 2011. High expression of p300 in human breast cancer correlates with tumor recurrence and predicts patients adverse prognosis. Chin. J. Cancer Res. 23 (3), 3–9.

Yang, H., Pinello, C.E., Luo, J., Li, D., Wang, Y., Zhao, L.Y., Jahn, S.C., Saldanha, S.A., Planck, J., Geary, K.R., Ma, H., Law, B.K., Roush, W.R., Hodder, P., Liao, D., 2013. Small-molecule inhibitors of acetyltransferase p300 identified by high-throughput screening are potent anticancer agents. Mol. Cancer Ther. 2 (5), 610–620.

Zhou, J., Zhan, S., Tan, W., Cheng, R., Gong, H., Zhu, Q., 2014. p300 binds to and acetylates MTA2 to promote colorectal cancer cells growth. Biochem. Biophys. Res. Commun. 444, 387–390.

Please cite this article as: Fermento, M.E., et al., Inhibition of p300 suppresses growth of breast cancer. Role of p300 subcellular localization, Exp. Mol. Pathol. (2014), http://dx.doi.org/10.1016/j.yexmp.2014.09.019